Research Article | Vol. 29, No. 26 / 20 Dec 2021 / Optics Express 44146
Optics EXPRESS

Chiral/directional mode transfer based on a tunable non-Hermitian system

YICONG ZHANG,[1] WEIWEI LIU,[1,3] HUA LONG,[1] KAI WANG,[1] BING WANG,[1,4] AND PEIXIANG LU[1,2,5]

[1]*Wuhan National Laboratory for Optoelectronics and School of Physics, Huazhong University of Science and Technology, Wuhan 430074, China*
[2]*Hubei Key Laboratory of Optical Information and Pattern Recognition, Wuhan Institute of Technology, Wuhan 430205, China*
[3]*lwhust@hust.edu.cn*
[4]*wangbing@hust.edu.cn*
[5]*lupeixiang@hust.edu.cn*

Abstract: Exceptional points (EPs) of non-Hermitian systems are the degeneracies of both the eigenvalues and eigenvectors, which have led to a series of novel and counterintuitive physical effects. Adiabatically encircling the EP in parameter space could lead to chiral mode transfer in coupled waveguides. However, the fixed refractive index distribution in existing devices will confine the parametric loops and lay great limitations on the performances of the mode conversion. Herein, we theoretically propose a non-Hermitian system based on refractive index modulation of coupled liquid crystal (LC) waveguides, which allows for encircling the EP with tunable loops. As a result, chiral mode transfer is achieved with optimized performances at wide telecommunication wavelengths, including a high transfer efficiency (>80%). Moreover, the dynamic modulation of the refractive index enables a directional mode transfer which is solely dependent on the modulation direction, even with non-closing evolution routes. The tunable non-Hermitian system serves as a versatile platform for realizing tunable mode transfer processes with optimized performances, showing great promise for developing multifunctional non-Hermitian nanophotonic devices.

1. Introduction

Nonconservative physical systems containing gain or loss can be described by non-Hermitian Hamiltonians which feature complex eigenvalues and non-orthogonal eigenvectors [1–7]. Recently, non-Hermitian physics have drawn great research interests in optics, including microcavities [8–12], integrated waveguides [13–17], photonic lattice [18–20], and metasurfaces [21,22]. Different from the degeneracies in Hermitian systems, the eigenvalues and the corresponding eigenvectors of the non-Hermitian systems coalesce simultaneously under specific conditions, thus giving rise to the exceptional points (EPs) [3,23–28]. Interestingly, the EPs have led to series of counterintuitive and fascinating phenomena, such as light stopping [29], unidirectional reflectionless light propagation [30], electromagnetically induced transparency [31,32] and coherent perfect absorption [28], which have played important roles in light steering and show great potential for constructing nanophotonic devices with novel functionalities.

In the parameter space, EPs are represented as the branch points of the complex Riemann sheets. Tuning the parameters of the non-Hermitian system will cause the eigenvalues to move on the Riemann surface. In particular, the eigenvalues and the corresponding eigenstates will exchange while adiabatically encircling an EP due to the topological features of the Riemann sheets in the vicinity of EPs [15,17,27,33–36]. This unique physical property has created conditions to implement chiral mode switching with the output state solely dependent on the direction of the parameter loop regardless of the input state [15,37,38]. For examples, dynamically encircling the

#445064 https://doi.org/10.1364/OE.445064
Journal © 2021 Received 3 Oct 2021; revised 11 Nov 2021; accepted 12 Nov 2021; published 17 Dec 2021

Optics EXPRESS

EP for chiral mode switching was originally implemented in the microwave systems [17], which has also been extended to the on-chip platforms based on silicon-on-insulator (SOI) waveguides [13,39,40]. However, in current nanophotonic non-Hermitian systems, the static structural properties of the components have limited the performances of the chiral mode switching, which may lead to fixed encircling loops with low conversion efficiency. Therefore, to construct a tunable non-Hermitian system is highly desirable for realizing modulated parameter loops in the vicinity of the EP, as well as achieving mode transfer with optimized performances.

In this work, we theoretically propose a tunable non-Hermitian system based on the electric-optic modulation of coupled liquid crystal (LC) waveguides, to realize tunable mode transfer in the optical telecommunication band. LC is advantageous for fabricating nanophotonic devices with tunable refractive index [41,42]. By applying variable voltages along the coupled LC waveguides, dynamically encircling the EP of the non-Hermitian system is realized to obtain the chiral mode switching between the odd and even modes. Taking advantages of the tunable non-Hermitian system, the evolution can be modulated to optimize the performances of the mode transfer for specific routes, thus achieving a high transfer efficiency (>80%) in a wide range of the wavelengths. Moreover, the dynamic modulation of the refractive index of the LC waveguides allows for designing non-closing routes without encircling the EP of the non-Hermitian system, which indicates that the topological feature of the parametric evolution still keeps and the mode transfer is solely dependent on the modulation direction (termed as "directional mode transfer").

2. Theoretical analysis and device design

In an optical system composed of two waveguides with weak coupling and loss applied on one of the waveguides, the coupled-mode equation can be written as [13,43,44]

$$-i\frac{d}{dz}\begin{bmatrix} a_1(z) \\ a_2(z) \end{bmatrix} = \begin{bmatrix} \alpha_1 & C \\ C & \alpha_2 + i\gamma \end{bmatrix}\begin{bmatrix} a_1(z) \\ a_2(z) \end{bmatrix} = H\begin{bmatrix} a_1(z) \\ a_2(z) \end{bmatrix}, \tag{1}$$

where $\alpha_{1,2}$ represent the effective mode indices, and γ is the loss coefficient of the second waveguide. C stands for the coupling coefficient between the waveguides. $a_1(z)$ and $a_2(z)$ are the amplitudes of the modes in the individual waveguides related to the propagation distance. The eigenvalues of the Hamiltonian matrix H are expressed as

$$E_{1,2} = \frac{\alpha_1 + \alpha_2 + i\gamma \pm \sqrt{[\alpha_1 - (\alpha_2 + i\gamma)]^2 + 4C^2}}{2}. \tag{2}$$

In particular, the eigenvalues and the eigenvectors will simultaneously coalesce at the EP, where $\Delta\alpha = \alpha_1 - \alpha_2 = 0$ and $C = \gamma/2$.

Here we demonstrate the tunable non-Hermitian system consisted of coupled LC waveguides operating in the transverse-electric (TE) modes. Figure 1(a) depicts the schematic of the designed device consisting of LC waveguides. The inset shows the E_x profiles of the odd and even modes. Quartz is used as the substrate ($n_{\text{Quartz}} = 1.50$). The LC is filled into the channels fabricated in the polymethyl methacrylate (PMMA) film with a thickness of 800 nm ($n_{\text{PMMA}} = 1.4807$). The width of the LC waveguides is set as $w_{\text{LC}} = 1200$ nm to ensure that only the fundamental mode is permitted. The gap between the two LC waveguides varies along the direction of propagation as $g(z) = g_0 - \Delta g\cos(2\pi z/L)$, where $g_0 = 800$ nm and $\Delta g = 400$ nm. The refractive index of LC waveguide 1 (WG1) can be tunable by an external electric field, $n_1(z) = 1.67 - \Delta n_1 \sin(2\pi z/L)$, and the refractive index of waveguide 2 (WG2) is fixed at $n_2 = 1.67$. The refractive index of the LC waveguide can be also modulated in segmentations, as detailed in Supplement 1. To introduce loss to LC WG2, a chromium film with width of 150 nm and thickness of 10 nm is deposited on the top of the waveguide. The corresponding loss coefficient is determined to be $\gamma = 0.0061$.

Optics EXPRESS

To guarantee adiabatic evolution, the length L of the waveguides is set to be 100 μm to make $n_1(z)$ and $g(z)$ varies slowly [13,17,39]. Figure 1(b) shows the encircling loops on the parameter space for various modulation amplitudes of the refractive index of WG1. The EP is located at $n_1 = 1.67$ and $g = 1140$ nm. The starting/end point is set on the line where the imaginary parts of the two eigenvalues coalesce to ensure that no more than one non-adiabatic transition (NAT) occurs for simplicity [15,34,45,46]. As the propagation distance increases, the corresponding $\Delta\alpha$ at 1550 nm are plotted in Fig. 1(c). Injections from the left ($z = 0$) and from the right ($z = L$) side of the waveguides respectively correspond to the clockwise (CW) and counterclockwise (CCW) directions in the encircling loops in Fig. 1(b).

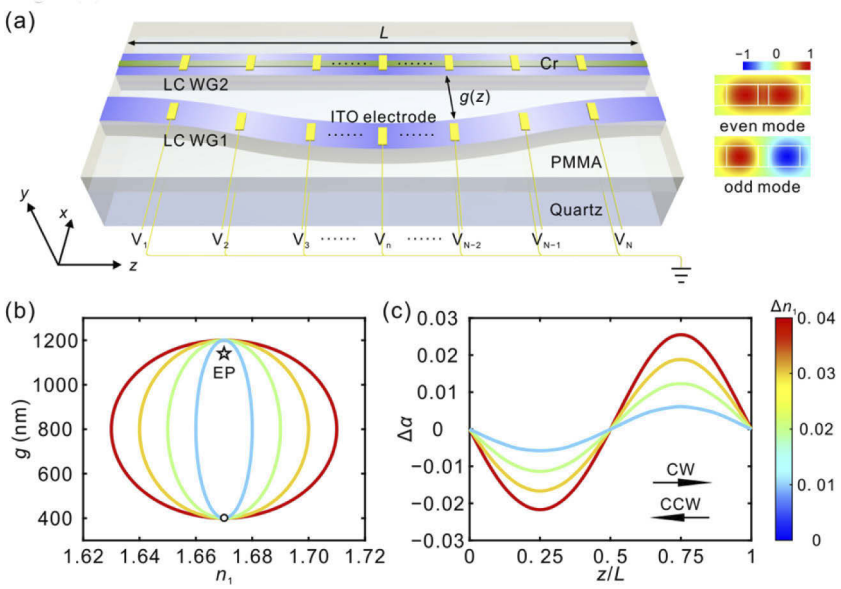

Fig. 1. (a) Scheme of the LC waveguide doublet and the profiles of the odd and even eigenmodes at both ends of the waveguides. (b) Parameter space of the system constituted by the refractive index of LC WG1 and the gap. The circle and the star mark the starting/end point of the loop and the EP. The parameter loops with $\Delta n_1 = 0.01$, 0.02, 0.03 and 0.04 are plotted for example. (c) Calculated effective mode index contrast $\Delta\alpha$ between LC WG1 and WG2 along the z-axis corresponding to the loops shown in (b). Propagations along $+z$ and $-z$ directions correspond to clockwise (CW) and counterclockwise (CCW) loops respectively.

To make a clear manifestation of the evolution of the eigenvalues, the Riemann surface in the parameter space composed of $\Delta\alpha$ and C and the corresponding trajectories of eigenvalues are illustrated in Fig. 2 (Δn_1 is set to be 0.04 for example). The real parts of eigenvalues represent the effective mode index while the imaginary parts represent the corresponding effective loss coefficients of the supermodes. The line on the upper sheet of the Riemann surfaces stands for the even mode, while that on the lower sheet stands for the odd mode. The parts of the Riemann sheets with higher loss are plotted in red and those with lower loss are plotted in green respectively. The field distribution at each propagation distance in the device can be expressed as the superposition of two eigenmodes [15,45,47]

$$|\psi(z)\rangle = A_h(z)|\varphi_h(z)\rangle + A_l(z)|\varphi_l(z)\rangle, \tag{3}$$

where the subscripts h and l represent the eigenmode with the higher and lower loss respectively. The trajectories are plotted on the red (green) sheet of the Riemann surfaces when $|A_h| > |A_l|$ ($|A_h| < |A_l|$), indicating that the higher-loss (lower-loss) mode dominates in the system. The

Optics EXPRESS

encircling process is adiabatic and stable when the state evolves on the lower-loss Riemann sheet. However, when the state evolves into the higher-loss Riemann sheet, the encircling process becomes unstable and an NAT may occur to lead the state to evolve towards the stable lower-loss Riemann sheet again [15,34–36,45,47]. This behavior is represented as the trajectory jumps from the higher-loss sheet to the lower-loss sheet. As a result, the eigenmode with the lower loss always dominates at the output and the final field distribution depends on the direction of the encircling loop. Figures 2(a)–2(d) show the trajectories of state evolution on the Riemann sheets of the real parts of eigenvalues, where the odd mode and even mode are injected from the left side and the right side respectively. According to the Riemann sheets and the trajectories, the output is expected to be dominated by the even mode for the CW loops and and odd mode for the CCW loops respectively, regardless of the input mode.

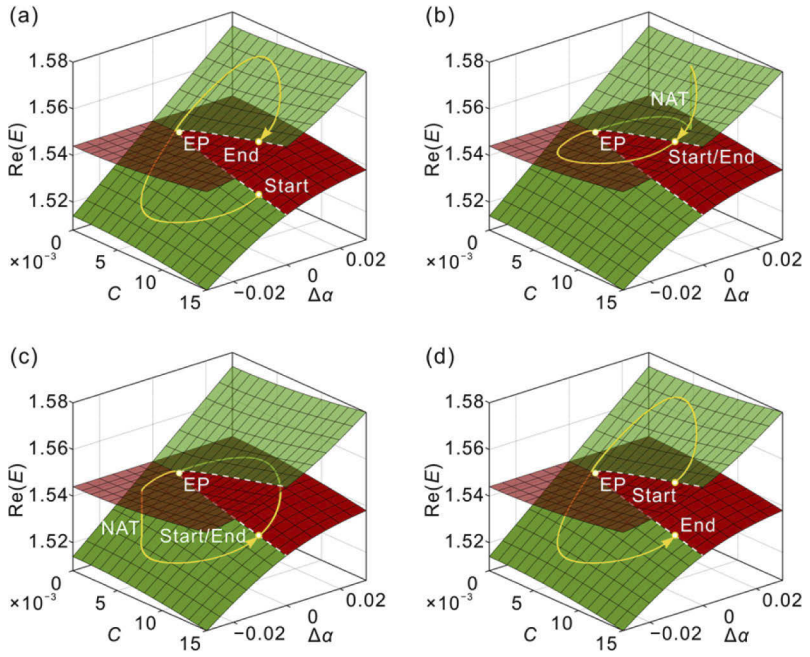

Fig. 2. Riemann sheets in the ($\Delta\alpha$, C) space. The green and red sheets represent the eigenvalues with lower and higher imaginary parts respectively. The yellow curves represent the trajectories for injecting (a) odd mode with CW loop, (b) even mode with CW loop, (c) odd mode with CCW loop and (d) even mode with CCW loop, respectively.

3. Results and discussions

3.1. Encircling the EP for chiral mode transfer with optimized performances

To demonstrate the chiral mode transfer, we simulate the field distribution of the coupled LC waveguides using full-wave 3D simulation in Comsol Multiphysics. We demonstrated that the anisotropy of the LC waveguide has little effect on the mode distribution (Section 2, Supplement 1), and an isotropic refractive index was utilized in the simulation. Figures 3(a)–3(d) show the calculated field distributions (E_x) for the CW and CCW encircling loops, with the odd and even mode incidence respectively. The modulated amplitude of the refractive index of WG1 is set to be $\Delta n_1 = 0.04$. For the CW loop, the even mode is always obtained at the output, regardless whether the odd mode or the even mode is injected from the left side of the waveguides (Figs. 3(a)–3(b)). On the contrary, for the CCW loop, the odd mode is always obtained at the

Optics EXPRESS

output (Figs. 3(c)–3(d)). Therefore, the simulation results indicate that the output mode is solely dependent on the direction of the encircling loop, regardless of the input mode. This result is consistent with the theoretical predictions, which demonstrate the chiral mode transfer between the eigenmodes of the coupled waveguides.

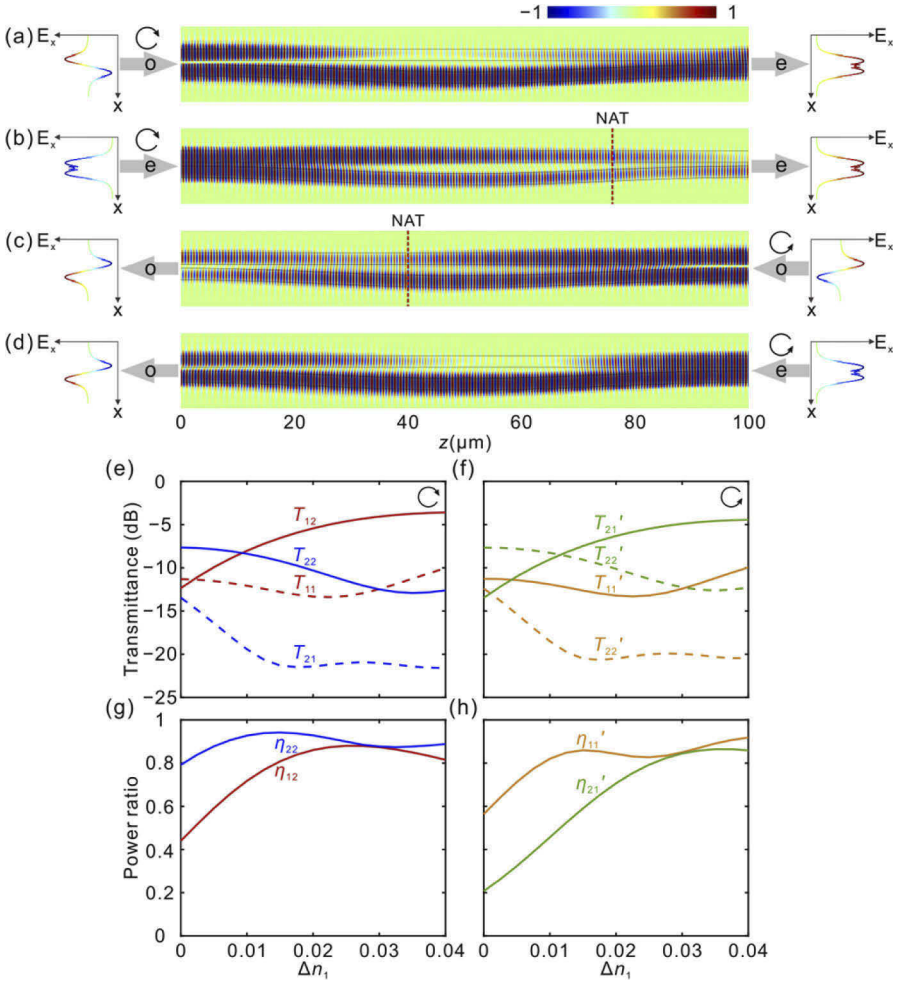

Fig. 3. (a)-(d) Numerically simulated field distributions (E_x) in the LC waveguides at 1550 nm with different encircling directions and injections. (a) The odd mode with CW loop, (b) even mode with CW loop, (c) odd mode with CCW loop, and (d) even mode with CCW loop. The input modes and the dominant modes at the output are marked with "o" for odd modes and "e" for even modes. The positions of NATs are marked by the red dashed lines in (b) and (c). Calculated transmittance for (e) CW loop, (f) CCW loop. The corresponding power ratio as Δn_1 varies for (g) CW loop, and (h) CCW loop. The solid curves in (e), (f) represent the transmittance of the predicted dominant modes at the output while the dashed curves represent the transmittance of the other. The arrows represent the corresponding encircling directions in the parameter space of (n_1, g).

The light transmittance and mode transfer efficiency are vital to characterize the performance of the chiral mode transfer. The mode transmittance, T_{mn} (T_{mn}'), is defined as the transmittance from input mode m to output mode n for the CW (CCW) loop. The mode transmittance can be calculated with $T_{\mathrm{mn}} = |\mathrm{A}_{1(2)}|^2 P_{\mathrm{out}}/P_{\mathrm{in}}$, where P_{in} and P_{out} refer to the input and output powers,

Optics EXPRESS

respectively, and $A_{1(2)}$ is the normalized amplitude of the odd (even) mode at the output terminal. Figures 3(e) and 3(f) present the mode transmittance at 1550 nm versus Δn_1, which corresponds to the encircling loops plotted in Fig. 1(b). We can observe that the transmittance of the even (odd) mode is always larger than that of the odd (even) mode for the CW (CCW) encircling loop within the range of $\Delta n_1 > 0.012$, which indicates that the even (odd) mode dominates at the output for the CW (CCW) encircling loop. For $\Delta n_1 < 0.012$, there is a slight discrepancy between T_{1n}, T_{2n}' and the theoretical results, which is due to the weak coupling between eigenstates caused by the small modulation range of refractive index. The mode transfer efficiency for the CW (CCW) encircling is defined as $\eta_{m2} = T_{m2}/(T_{m1}+T_{m2})$ ($\eta_{m1}' = T_{m1}'/(T_{m1}'+T_{m2}')$), i.e., the power ratio of the output modes. Figures 3(g) and 3(h) present the calculated power ratios for the two encircling directions respectively. All the results show that the power ratios are larger than 0.8 within the range $0.025 < \Delta n_1 < 0.04$, indicating a high mode transfer efficiency. In particular, taking advantages of the tunable refractive index of the LC waveguides, the encircling trajectory of the non-Hermitian system can be modulated to achieve the highest mode transfer efficiency for different encircling directions and input modes, which suggests great superiority compared with the static non-Hermitian systems.

We also calculated the spectral response of the LC-waveguide based non-Hermitian system. Figure 4 shows the mapping of transfer efficiencies as functions of Δn_1 and wavelength. In the simulation, the frequency dispersion of the LC waveguide can be negligible (Section 3, Supplement 1) [48]. For the CW encircling loop with odd and even modes injected, as shown in Figs. 4(a) and 4(b) respectively, η_{m2} is always above 0.7 with $0.017 < \Delta n_1 < 0.033$ in the whole C + L communication bands, indicating that the even mode dominates at the output. Figures 4(c) and 4(d) show that under the condition $0.021 < \Delta n_1 < 0.04$, η_{m1}' is also above 0.7 at wavelengths below 1595 nm, suggesting that the output is dominated by the odd mode. The calculated results show an excellent performance of the chiral mode transfer for the optical communication applications. Moreover, the highest transfer efficiency at a specific wavelength

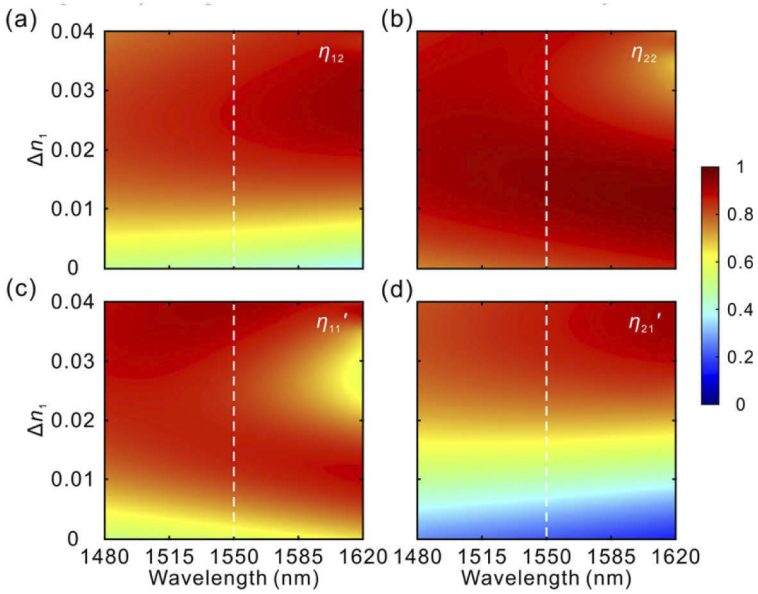

Fig. 4. Simulated spectral response of the transfer efficiency as Δn_1 varies for injecting (a) odd mode with CW loop, (b) even mode with CW loop, (c) odd mode with CCW loop, and (d) even mode with CCW loop. The white dashed lines mark the wavelength at 1550 nm.

Optics EXPRESS

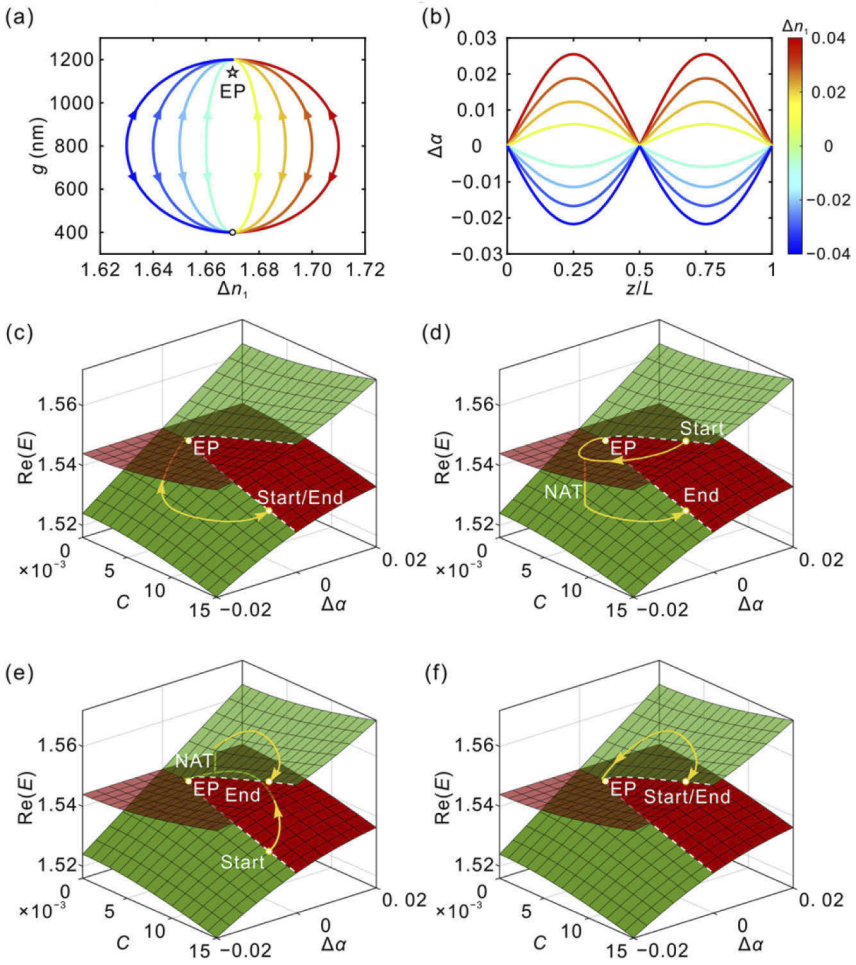

Fig. 5. (a) Arched parameter trajectories for various Δn_1 in the (n_1, g) space without encircling the EP. The start/end point of the trajectories is marked by the black circle and the evolution directions of the parameters are shown by the arrows. (b) Plot of $\Delta\alpha$ as functions of the propagation distance, for different Δn. (c)-(f) Riemann sheets with the parameter paths corresponding to the arched trajectories in (a). $\Delta n_1 = -0.02$ for (c)(d), and $\Delta n_1 = 0.02$ for (e)(f), respectively.

for every mode transfer process can be achieved respectively via appropriate refractive index modulation amplitude, which demonstrates the optimization property of the designed device.

3.2. *Modulation-induced directional mode transfer without encircling the EP*

The tunable non-Hermitian system provides a versatile platform to achieve flexible paths to investigate the mode evolution. Here we design some non-closing paths to investigate the mode transfer without encircling the EP. The refractive index of LC WG1 is defined as $n_1(z) = 1.67+\Delta n_1|\sin(2\pi z/L)|$, while that of LC WG2 is still kept to be 1.67. Figure 5(a) shows the arched trajectories in the parameter space for various modulation amplitudes of the refractive index, and Fig. 5(b) plots the corresponding $\Delta\alpha$ as a function of z. For each Δn_1, the evolution paths move around the EP and return back to the start in the same trajectory. As shown in Fig. 5(c), for a negative Δn_1, the odd mode injection will lead to an evolution trajectory along the

Optics EXPRESS

low-loss (green) sheet. As a result, no NAT occurs, and the input mode can directly propagate to the output terminal. However, the even mode injection will lead to an evolution trajectory along the high-loss (red) sheet (Fig. 5(d)). After z reaches $L/2$, the trajectories retrace in the vicinity of the EP. As a result, the mode would still experience an NAT in the evolution process even though the EP is not encircled, thus leading to a transfer from the even mode to the odd mode. Similarly, for a positive Δn_1, the odd mode injection could experience NAT and transfer to the even mode (Fig. 5(e)), while the even mode injection can directly propagate to the output terminal (Fig. 5(f)). Although the parameter trajectory that does not encircle but passes in the vicinity of the EP, the topological feature still remains, because the output mode is solely dependent on the modulation direction of the refractive index, regardless of the input mode. Moreover, the transfer between the odd and even modes here is attributed to the NAT, which is different from the situation by encircling the EP.

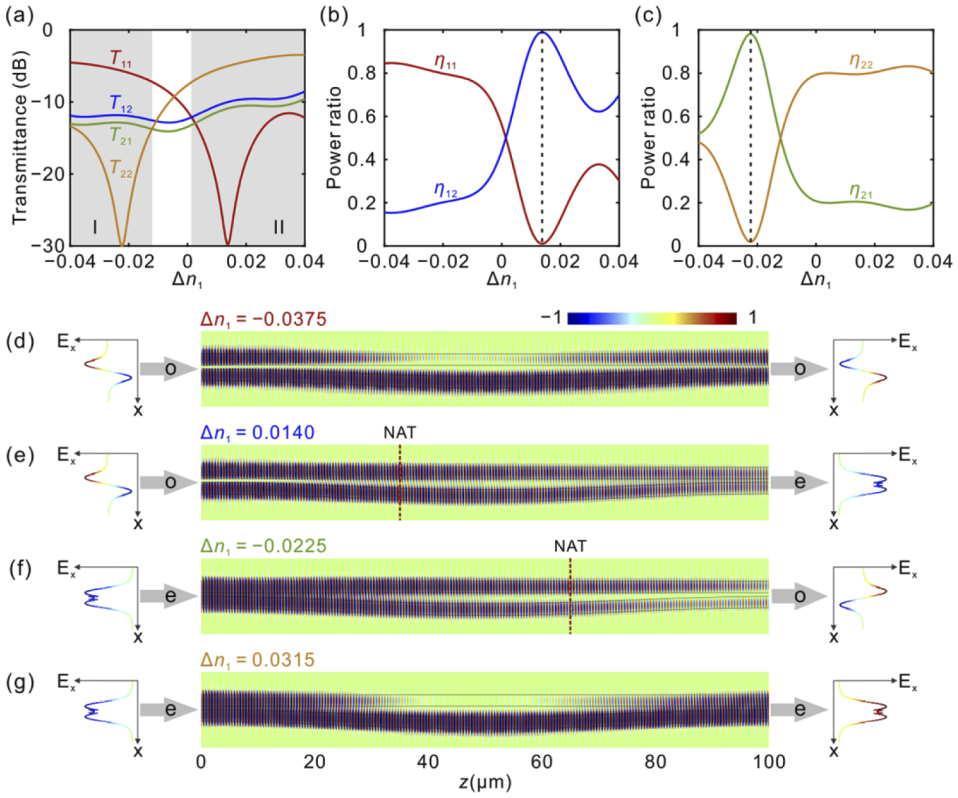

Fig. 6. (a) The simulated transmittance as a function of Δn_1. The grey regions I and II mark the range of Δn_1 which guarantees that the odd and even mode dominate at the output respectively regardless of the initial state. (b)(c) The power ratio at the output with the odd and the even mode injected respectively. The black dashed lines mark $\Delta n_1 = 0.0140$ and -0.0225 where η_{12} and η_{21} reach the maximum respectively. (d)-(f) Numerically simulated field distributions (E_x) in the LC waveguides at 1550 nm with the arched parameter trajectories where (d) $\Delta n_1 = -0.0375$, (e) $\Delta n_1 = 0.0140$, (f) $\Delta n_1 = -0.0225$ and (g) $\Delta n_1 = 0.0315$, to achieve the maximum mode transfer efficiency. The selected values of Δn_1 are given in the same color as the curves in Fig. 6(b) and 6(c), which corresponds to maximum η_{11}, η_{12}, η_{21} and η_{22} respectively. The positions of NATs are marked by the red dashed lines in (e) and (f).

Optics EXPRESS

Figure 6(a) presents the calculated mode transmittances as functions of Δn_1. For $\Delta n_1 < -0.012$ (region I), T_{m1} is always larger than T_{m2}, suggesting that the input is dominantly transferred into the odd mode. In contrast, for $\Delta n_1 > 0.002$ (region II), the input is dominantly transferred into the even mode, which is consistent with the theoretical predictions. We also notice that the propagation processes without mode transfer possess the lower loss, i.e., T_{11} and T_{22} act as the highest transmittance in region I and II respectively, which is due to that both the parameter evolution processes are dominated by the stable eigenstates. Figures 6(b) and 6(c) show the corresponding power ratios for odd and even mode injections respectively, where the peak value of η_{12} and η_{21} located at $\Delta n_1 = 0.0140$ and $\Delta n_1 = -0.0225$ are respectively marked by the black dashed lines. In particular, the mode transfer efficiency can be up to ~100%, which exhibits further improvement compared with the corresponding mode transfer efficiencies (η_{12} and η_{21}') in Figs. 3(g) and 3(h). Therefore, an efficient mode transfer can still be realized even though the EP is not encircled by the arched parameter trajectory.

The field distributions for arched parameter trajectories are calculated to demonstrate the mode transfer without encircling the EP, as presented in Figs. 6(d)–6(g). According to Figs. 6(b) and 6(c), Δn_1 is respectively set to be −0.0375, 0.0140, −0.0225 and 0.0315 to achieve optimized power ratios (η_{11}, η_{12}, η_{21}, η_{22}). One can observe that the output is dominated by the odd mode for the first and third case while the even mode for the second and forth case, as analyzed above. The evolution is due to the topological feature of the Riemann sheets, and the NAT in the vicinity of the EP remains strong even without encircling the EP [14,49]. Therefore, we can conclude that the existence of the NAT is not strictly dependent on the parameter loop encircling the EP. Though chiral mode transfers have been demonstrated by closing loops even without encircling the EPs, the transfer processes were similar to that with encircling the EPs [14,49]. In contrast, the non-closing arched paths here enable to realize a directional mode transfer, and the output can be flexibly tuned through refractive index modulation in an individual device. The utilization of the tunable non-Hermitian system and the arched parameter trajectory not only demonstrate the feasibility of realizing directional mode transfer without encircling the EP, but also offer an effective approach to achieving a high mode transfer efficiency.

4. Conclusions

In summary, we have theoretically proposed a non-Hermitian system based on coupled liquid crystal (LC) waveguides to realize tunable mode transfer for optical communications. The refractive index modulation along the coupled LC waveguides enables to realize chiral mode transfer by dynamically encircling the EP of the non-Hermitian system. In particular, the performances of the mode transfer can be optimized to obtain a high transfer efficiency (>80%) in a wide range of the wavelengths. Moreover, the directional mode transfer is realized even without encircling the EP of the non-Hermitian system. The tunable non-Hermitian system provides a versatile platform for realizing tunable mode transfer processes with optimized performances, which shows great promise for developing multifunctional non-Hermitian nanophotonic devices.

Funding. National Natural Science Foundation of China (11674117, 11804109, 12021004).

Disclosures. The authors declare no conflicts of interest.

Data availability. Data underlying the results presented in this paper are not publicly available at this time but may be obtained from the authors upon reasonable request.

Supplemental document. See Supplement 1 for supporting content.

References

1. M. V. Berry, "Physics of nonhermitian degeneracies," Czech. J. Phys. **54**(10), 1039–1047 (2004).
2. I. Rotter, "A non-Hermitian Hamilton operator and the physics of open quantum systems," J. Phys. A: Math. Theor. **42**(15), 153001 (2009).

Optics EXPRESS

3. H.-Z. Chen, T. Liu, H.-Y. Luan, R.-J. Liu, X.-Y. Wang, X.-F. Zhu, Y.-B. Li, Z.-M. Gu, S.-J. Liang, H. Gao, L. Lu, L. Ge, S. Zhang, J. Zhu, and R.-M. Ma, "Revealing the missing dimension at an exceptional point," Nat. Phys. **16**(5), 571–578 (2020).
4. E. J. Bergholtz, J. C. Budich, and F. K. Kunst, "Exceptional topology of non-Hermitian systems," Rev. Mod. Phys. **93**(1), 015005 (2021).
5. E. Hernández, A. Jáuregui, and A. Mondragón, "Exceptional points and non-Hermitian degeneracy of resonances in a two-channel model," Phys. Rev. E **84**(4), 046209 (2011).
6. L. Feng, R. El-Ganainy, and L. Ge, "Non-Hermitian photonics based on parity-time symmetry," Nat. Photonics **11**(12), 752–762 (2017).
7. R. El-Ganainy, K. G. Makris, M. Khajavikhan, Z. H. Musslimani, S. Rotter, and D. N. Christodoulides, "Non-Hermitian physics and PT symmetry," Nat. Phys. **14**(1), 11–19 (2018).
8. M. J. Grant and M. J. F. Digonnet, "Rotation sensitivity and shot-noise-limited detection in an exceptional-point coupled-ring gyroscope," Opt. Lett. **46**(12), 2936–2939 (2021).
9. J. Wen, X. Jiang, L. Jiang, and M. Xiao, "Parity-time symmetry in optical microcavity systems," J. Phys. B: At., Mol. Opt. Phys. **51**(22), 222001 (2018).
10. W. Chen, Ş. Kaya Özdemir, G. Zhao, J. Wiersig, and L. Yang, "Exceptional points enhance sensing in an optical microcavity," Nature **548**(7666), 192–196 (2017).
11. B. Peng, Ş. K. Özdemir, F. Lei, F. Monifi, M. Gianfreda, G. L. Long, S. Fan, F. Nori, C. M. Bender, and L. Yang, "Parity-time-symmetric whispering-gallery microcavities," Nat. Phys. **10**(5), 394–398 (2014).
12. S.-B. Lee, J. Yang, S. Moon, S.-Y. Lee, J.-B. Shim, S. W. Kim, J.-H. Lee, and K. An, "Observation of an exceptional point in a chaotic optical microcavity," Phys. Rev. Lett. **103**(13), 134101 (2009).
13. Q. Liu, S. Li, B. Wang, S. Ke, C. Qin, K. Wang, W. Liu, D. Gao, P. Berini, and P. Lu, "Efficient mode transfer on a compact silicon chip by encircling moving exceptional points," Phys. Rev. Lett. **124**(15), 153903 (2020).
14. Q. Liu, J. Liu, D. Zhao, and B. Wang, "On-chip experiment for chiral mode transfer without enclosing an exceptional point," Phys. Rev. A **103**(2), 023531 (2021).
15. X.-L. Zhang, S. Wang, B. Hou, and C. T. Chan, "Dynamically encircling exceptional points: in situ control of encircling loops and the role of the starting point," Phys. Rev. X **8**(2), 021066 (2018).
16. A. U. Hassan, B. Zhen, M. Soljačić, M. Khajavikhan, and D. N. Christodoulides, "Dynamically encircling exceptional points: exact evolution and polarization state conversion," Phys. Rev. Lett. **118**(9), 093002 (2017).
17. J. Doppler, A. A. Mailybaev, J. Böhm, U. Kuhl, A. Girschik, F. Libisch, T. J. Milburn, P. Rabl, N. Moiseyev, and S. Rotter, "Dynamically encircling an exceptional point for asymmetric mode switching," Nature **537**(7618), 76–79 (2016).
18. L.-Z. Tang, G.-Q. Zhang, L.-F. Zhang, and D.-W. Zhang, "Localization and topological transitions in non-Hermitian quasiperiodic lattices," Phys. Rev. A **103**(3), 033325 (2021).
19. X.-S. Li, P.-P. Huang, J. He, L.-L. Zhang, and W.-J. Gong, "Fano effect in a one-dimensional photonic lattice with side-coupled P T-symmetric non-Hermitian defects," Opt. Express **28**(6), 8560–8573 (2020).
20. M. Pan, H. Zhao, P. Miao, S. Longhi, and L. Feng, "Photonic zero mode in a non-Hermitian photonic lattice," Nat. Commun. **9**(1), 1308 (2018).
21. M. Kang, T. Zhang, B. Zhao, L. Sun, and J. Chen, "Chirality of exceptional points in bianisotropic metasurfaces," Opt. Express **29**(8), 11582–11590 (2021).
22. S. H. Park, L. Sung-Gyu, S. Baek, T. Ha, S. Lee, M. Bumki, S. Zhang, M. Lawrence, and T.-T. Kim, "Observation of an exceptional point in a non-Hermitian metasurface," Nanophotonics **9**(5), 1031–1039 (2020).
23. T. Wu, W. Zhang, H. Zhang, S. Hou, G. Chen, R. Liu, C. Lu, J. Li, R. Wang, P. Duan, J. Li, B. Wang, L. Shi, J. Zi, and X. Zhang, "Vector exceptional points with strong superchiral fields," Phys. Rev. Lett. **124**(8), 083901 (2020).
24. W. D. Heiss, "The physics of exceptional points," J. Phys. A: Math. Theor. **45**(44), 444016 (2012).
25. X.-L. Zhang, S. Wang, W.-J. Chen, and C. T. Chan, "Exceptional points and symmetry recovery in a two-state system," Phys. Rev. A **96**(2), 022112 (2017).
26. M.-A. Miri and A. Alù, "Exceptional points in optics and photonics," Science **363**(6422), eaar7709 (2019).
27. Ş. K. Özdemir, S. Rotter, F. Nori, and L. Yang, "Parity-time symmetry and exceptional points in photonics," Nat. Mater. **18**(8), 783–798 (2019).
28. C. Wang, R. Sweeney William, A. D. Stone, and L. Yang, "Coherent perfect absorption at an exceptional point," Science **373**(6560), 1261–1265 (2021).
29. T. Goldzak, A. A. Mailybaev, and N. Moiseyev, "Light stops at exceptional points," Phys. Rev. Lett. **120**(1), 013901 (2018).
30. Y. Huang, Y. Shen, C. Min, S. Fan, and G. Veronis, "Unidirectional reflectionless light propagation at exceptional points," Nanophotonics **6**(5), 977–996 (2017).
31. C. Wang, X. Jiang, G. Zhao, M. Zhang, C. W. Hsu, B. Peng, A. D. Stone, L. Jiang, and L. Yang, "Electromagnetically induced transparency at a chiral exceptional point," Nat. Phys. **16**(3), 334–340 (2020).
32. T.-X. Lu, H. Zhang, Q. Zhang, and H. Jing, "Exceptional-point-engineered cavity magnomechanics," Phys. Rev. A **103**(6), 063708 (2021).
33. C. Dembowski, B. Dietz, H. D. Gräf, H. L. Harney, A. Heine, W. D. Heiss, and A. Richter, "Encircling an exceptional point," Phys. Rev. E **69**(5), 056216 (2004).

Optics EXPRESS

34. T. J. Milburn, J. Doppler, C. A. Holmes, S. Portolan, S. Rotter, and P. Rabl, "General description of quasiadiabatic dynamical phenomena near exceptional points," Phys. Rev. A **92**(5), 052124 (2015).
35. H. Wang, S. Assawaworrarit, and S. Fan, "Dynamics for encircling an exceptional point in a nonlinear non-Hermitian system," Opt. Lett. **44**(3), 638–641 (2019).
36. X.-L. Zhang, J.-F. Song, C. T. Chan, and H.-B. Sun, "Distinct outcomes by dynamically encircling an exceptional point along homotopic loops," Phys. Rev. A **99**(6), 063831 (2019).
37. B. Peng, Ş. K. Özdemir, M. Liertzer, W. Chen, J. Kramer, H. Yılmaz, J. Wiersig, S. Rotter, and L. Yang, "Chiral modes and directional lasing at exceptional points," Proc. Natl. Acad. Sci. **113**(25), 6845–6850 (2016).
38. A. Li, J. Dong, J. Wang, Z. Cheng, J. S. Ho, D. Zhang, J. Wen, X.-L. Zhang, C. T. Chan, A. Alù, C.-W. Qiu, and L. Chen, "Hamiltonian hopping for efficient chiral mode switching in encircling exceptional points," Phys. Rev. Lett. **125**(18), 187403 (2020).
39. J. W. Yoon, Y. Choi, C. Hahn, G. Kim, S. H. Song, K.-Y. Yang, J. Y. Lee, Y. Kim, C. S. Lee, J. K. Shin, H.-S. Lee, and P. Berini, "Time-asymmetric loop around an exceptional point over the full optical communications band," Nature **562**(7725), 86–90 (2018).
40. S.-R. Yang, X.-L. Zhang, and H.-B. Sun, "Design of a non-Hermitian on-chip mode converter using phase change materials," Opt. Lett. **45**(16), 4630–4633 (2020).
41. D.-P. Cai, S.-C. Nien, H.-K. Chiu, C.-C. Chen, and C.-C. Lee, "Electrically tunable liquid crystal waveguide attenuators," Opt. Express **19**(12), 11890–11896 (2011).
42. C.-C. Shih, "Voltage-controllable liquid crystal waveguide," Optik **127**(4), 2393–2395 (2016).
43. W.-P. Huang and J. Mu, "Complex coupled-mode theory for optical waveguides," Opt. Express **17**(21), 19134–19152 (2009).
44. J. Xu and Y. Chen, "General coupled mode theory in non-Hermitian waveguides," Opt. Express **23**(17), 22619–22627 (2015).
45. X.-L. Zhang, T. Jiang, and C. T. Chan, "Dynamically encircling an exceptional point in anti-parity-time symmetric systems: asymmetric mode switching for symmetry-broken modes," Light: Sci. Appl. **8**(1), 88 (2019).
46. X.-L. Zhang and C. T. Chan, "Hybrid exceptional point and its dynamical encircling in a two-state system," Phys. Rev. A **98**(3), 033810 (2018).
47. X.-L. Zhang and C. T. Chan, "Dynamically encircling exceptional points in a three-mode waveguide system," Commun. Phys. **2**(1), 63 (2019).
48. M. Ma, S. Li, X. Jing, and H. Chen, "Refractive indices of liquid crystal E7 depending on temperature and wavelengths," Opt. Eng. **56**(11), 117109 (2017).
49. A. U. Hassan, G. L. Galmiche, G. Harari, P. LiKamWa, M. Khajavikhan, M. Segev, and D. N. Christodoulides, "Chiral state conversion without encircling an exceptional point," Phys. Rev. A **96**(5), 052129 (2017).